JTTEE5 17:410–419
DOI: 10.1007/s11666-008-9184-2
1059-9630/$19.00 © ASM International

Peer Reviewed

# Influence of a Sealing Treatment on the Behavior of Plasma-Sprayed Alumina Coatings Operating in Extreme Environments

*Geoffroy Berard, Patrice Brun, Jacques Lacombe, Ghislain Montavon, Alain Denoirjean, and Guy Antou*

*(Submitted October 8, 2007; in revised form February 7, 2008)*

**In numerous applications developed at the Commissariat à l'Energie Atomique, Direction de l'Energie Nucléaire (CEA-DEN, *French Atomic Agency, Atomic Energy Department*), particularly those encountered in the processing of nuclear wastes, metallic components are subjected to extreme environments in service, in terms, for example, of ageing at moderated temperature (several months at about 300 °C) coupled to thermal shocks (numerous cycles up to 850 °C for a few seconds and a few ones up to 1500 °C) under a reactive environment made of a complex mixture of acid vapors in the presence of an electric field of a few hundred volts and a radioactive activity. Alumina plasma-sprayed coatings manufactured with feedstock of different particle size distributions, graded alumina-titania coatings, and phosphate-sealed alumina coatings were investigated to improve the properties of metallic substrates operating in such extreme environments. The effects of particle size distribution, phosphate sealant, and graded titania additions on the dielectric strength of the as-sprayed, thermally cycled and thermally aged coatings were investigated. Thermal ageing test was realized in furnace at 350 °C for 400 h and thermal shocks tests resulted from cycling the coating between 850 and 150 °C using oxyacetylene flame and compressed air-cooling. Alumina coating structures and phase content were characterized in parallel by scanning electron microscopy (SEM) coupled to image analysis and stereological protocols and X-ray diffractometry (XRD). The dielectric strength was assessed by measuring the breakdown voltage at 50 Hz during and after the thermal tests.**

**Keywords** dielectric coating, diffusion barrier, extreme environment, plasma spraying, porosity, thermal shock

## 1. Introduction

The increase in the lifetime of AISI 304L stainless steel structures, which are widely used in the nuclear industry, can enable new applications in extreme environments, particularly in the ones encountered in nuclear waste processing, where components experience long-term ageing (about 300 °C for several months) coupled to thermal shocks (numerous cycles up to 850 °C for a few seconds and a few ones up to 1500 °C) under a reactive environment made of a complex mixture of acid vapors in the presence of an electric field of a few hundred volts and a radioactive activity (higher than 10 MGy on a cumulated period of 4 years).

The aim of this work was to study the protection of AISI 304L substrates facing these coupled solicitations implementing atmospheric plasma-sprayed alumina coatings. Indeed, this technology seems very well adapted for applying coatings onto metallic components of large areas (a few square meters in the considered cases).

The selection of alumina as protective material results from its excellent intrinsic properties in regards with the solicitations in service: a good chemical inertia to acid products, an excellent dielectric behavior (breakdown voltage of about 3000 V under 50 Hz for a plasma-sprayed coating thickness of about 500 μm (Ref 1)), and good thermal insulation properties (thermal conductivity of about 5 W $m^{-1}$ $K^{-1}$ for plasma-sprayed alumina coatings (Ref 2)).

Nevertheless, ceramic plasma-sprayed coatings exhibit a pore network architecture that is connected to the substrate and which depends mostly upon operating spray parameters and feedstock characteristics (Ref 3-5). Such a connectivity results from the combination of unique features within the coating: (i) intralamellar cracks (i.e., parallel to the spray direction, in a first approximation, that is to say perpendicular to the substrate surface) resulting from residual stress relaxation within lamellae at their solidification and cooling, mostly; (ii) interlamellar

**Geoffroy Berard, Patrice Brun,** and **Jacques Lacombe**, Commissariat à l'Energie Atomique, Direction de l'Energie Nucléaire, VALRHO – Centre de Marcoule, 30207, Bagnols-sur-Ceze, France; and **Ghislain Montavon**, **Alain Denoirjean**, and **Guy Antou**, SPCTS – UMR CNRS 6638, Faculty of Sciences, University of Limoges, 123 Avenue Albert Thomas, 87060, Limoges Cedex, France. Contact e-mail: geoffroy.berard@mat.ensmp.fr.

cracks (perpendicular to the spray direction, in a first approximation, that is to say parallel to the substrate surface) resulting from stacking defects, stagnating vapors near to substrate during coating formation, desorption of absorbates or improper lamella flattening ratio; (iii) globular voids resulting mostly from stacking defects; and (iv) toric pores around unmolten particles or in-flight resolidified particles, if any. This lamellar microstructure with connected porosity can accommodate deformation and enhance the thermal insulation properties of the layers (Ref 6). On the opposite, this characteristic appears very detrimental for some coating properties in service since electrically conductive and/or corrosive solutions can percolate through the connected pore network, leading to the development of severe damages in the coating and at the coating/substrate interface consecutive to the propagation of electric arcs and to the corrosion of the substrate, or the bond coat if any.

Facing all thermal, chemical, and electrical constraints, a protective plasma-sprayed coating suitable for a long lifetime in some applications at the Commissariat à l'Energie Atomique, Direction de l'Energie Nucléaire (CEA-DEN, *French Atomic Agency, Atomic Energy Department*) needs to exhibit a non-connected pore network (i.e., gastight ceramic layer (Ref 7)).

Among several possible pre-treatments such as, for example, in situ treatments (i.e., laser remelting (Ref 8)), graded ceramic coatings (Ref 9) or post-treatments (i.e., shot-peening (Ref 10), laser remelting (Ref 11), annealing by adding of a second phase with a lower melting point (Ref 12), etc.), pore sealing permitting to densify the coating (Ref 13) appears in this context as a suitable technique, both from the economical and technical points of view.

The possible sealants for alumina coatings can be metals and metallic alloys deposited by electro-deposition (Ref 14), polymers (Ref 15), and inorganic solutions such as phosphate-based solutions (Ref 16). The sealing process using metallic and polymers was discarded because their properties are not adapted with the extreme environments considered in this study. Indeed, adding a metallic phase would considerably decrease the dielectric strength of the coating and polymers have poor thermal properties and radiation resistance in regard to the high temperatures and the high radioactive activity considered here. The sealing of plasma-sprayed alumina coatings by aluminum phosphate impregnation is the simplest technique in order to fill the connected porosity. The very complete studies of Ahmaniemi et al. (Ref 16) and Vippola et al. (Ref 17, 18) have shown the good compatibility of properties between alumina coating and aluminum phosphate sealant, allowing obtaining a coating with improved properties.

This procedure was applied on alumina coatings manufactured with feedstock of different particle size distributions and on alumina-based coatings with different graded titania additions. The coatings were applied on AISI 304L stainless steel substrates onto which a Ni-Al bond coat was applied by air plasma spraying (APS). This bond-coat nature was selected as a reference material for the purpose of this article, knowing that the final applications consider other specifically developed materials. In this study, it was nevertheless never observed that the nature of the bond coat modifies the ceramic layer characteristics and properties. The microstructure and the dielectric strength of these coatings were characterized before and after thermal tests by scanning electron microscopy (SEM) coupled to image analysis and stereological protocols, X-ray diffractometry (XRD), and breakdown voltage measurements.

## 2. Experimental Protocols

### 2.1 Substrates and Feedstock

Substrates were made of AISI 304L stainless steel button-type substrates of 25 mm in diameter and 6 mm in thickness that were drilled on their side at 3 mm from the surface to insert a thermocouple of 1 mm in diameter during the thermal shock tests. Prior to spraying, substrates were manually grit-blasted (i.e., $\alpha$-$Al_2O_3$ white corundum of 500 μm, average diameter) and degreased by immersion in acetone vapors. After grit-blasting, the substrates exhibited an average roughness (Ra (Ref 19)) of 4 μm, average value, and a peak-to-valley height (Rz (Ref 19)) of 32 μm, average value.

Coatings consisted in a 100-μm-thick metallic bond coat made of Ni-Al 5% by weight (Amdry 956, Sulzer-Metco, Wohlen, Switzerland) of particle size distribution ranging from 45 to 90 μm (supplier data) manufactured implementing air plasma spraying (APS) and in an alumina top coat of 200 μm thick (Medipur Medicoat, Mägenwil, Switzerland) of different particle size distributions (supplier data): +1 −10 μm, +5 −45 μm, +22 −45 μm, and +5 −20 μm. Graded alumina-titania coatings of 300 μm thick were made of several layers: the top coat made of alumina Medipur $Al_2O_3$ of particle size distribution +22 −45 μm and the intermediate layers made of (from top coat to substrate): alumina-titania 3% by weight (Amperit 742.3, H.C. Stark, Goslar, Germany), alumina-titania 13% by weight (Amperit 748.1, H.C. Stark, Goslar, Germany), or alumina-titania 40% by weight (Amperit 745.1), all of them exhibiting particle size distributions ranging from 22 to 45 μm (supplier data). The same Ni-Al bond coat was applied prior to ceramic layer spraying.

Table 1 displays the spray parameters used to manufacture these different layers. Table 2 synthesizes the different coating architectures that were considered. Figure 1 displays a typical as-sprayed architecture of pure alumina coatings. It is characterized by a lamellar structure and by its pore network made of cracks, delaminations, and globular pores. Figure 2 displays the typical architecture of an as-sprayed coating without bond coat and with a graded alumina-titania 60/40 first intermediate layer (50 μm, average thickness) and a graded alumina-titania 87/13 second intermediate layer (100 μm, average thickness) and a pure alumina top coat (130 μm, average thickness).

**Table 1 Operating spray parameters for bond and top coatings**

| | Top and graded titania coatings | Bond coat |
|---|---|---|
| Process | APS | APS |
| Feedstock | $Al_2O_3$, $Al_2O_3$-3$TiO_2$, $Al_2O_3$-13$TiO_2$, $Al_2O_3$-40$TiO_2$ | Ni-Al 95/5 |
| Spray gun (a) | Sulzer-Metco F4-type (a) | Sulzer-Metco F4-type (a) |
| Nozzle characteristic | 6 mm internal diameter anode | 6 mm internal diameter anode |
| Arc current intensity, A | 600 | 600 |
| Primary plasma gas flow rate (Ar), slpm | 46 | 55 |
| Secondary plasma gas flow rate ($H_2$), slpm | 14 | 9.4 |
| Spray distance, mm | 125 | 140 |
| Surrounding atmosphere | Air at atmospheric pressure | Air at atmospheric pressure |
| Powder feed rate, g $min^{-1}$ | 20 | 70 |
| Feedstock injection | Externally, injector diameter of 1.8 mm located 6 mm from the torch centerline axis and 4 mm downstream the torch exit | Externally, injector diameter of 1.8 mm located 6 mm from the torch centerline axis and 4 mm downstream the torch exit |
| Carrier gas flow rate (nature), slpm | 3.6 (Ar) | 3.5 (Ar) |

(a) Sulzer-Metco, Wohlen, Switzerland, formerly Sulzer and formerly Plasma-Technik

**Table 2 Description of the different coating architectures of the as-sprayed alumina coatings and references**

| Reference | A | B | C | D | E | F |
|---|---|---|---|---|---|---|
| Top coat | $Al_2O_3$ +1 −10 μm | $Al_2O_3$ +22 −45 μm | $Al_2O_3$ +5 −45 μm | $Al_2O_3$ +5 −20 μm | $Al_2O_3$ +22 −45 μm | $Al_2O_3$ +22 −45 μm |
| Intermediate layers | … | … | … | … | $Al_2O_3$-13$TiO_2$ $Al_2O_3$-40$TiO_2$ | $Al_2O_3$-3$TiO_2$ $Al_2O_3$-13$TiO_2$ |
| Bond coat | Ni-Al | Ni-Al | Ni-Al | Ni-Al | … | Ni-Al |

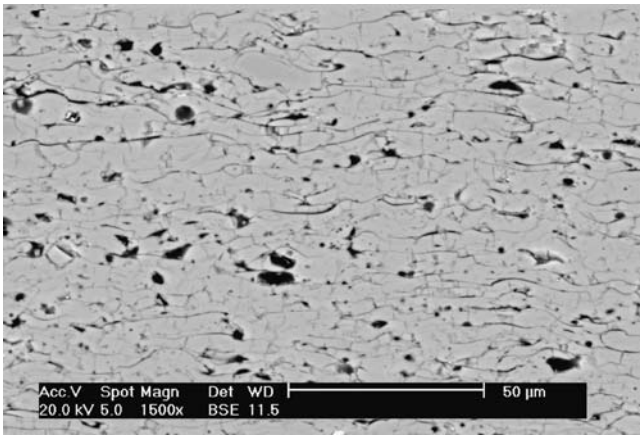


**Fig. 1** Typical as-sprayed architecture of pure alumina coatings

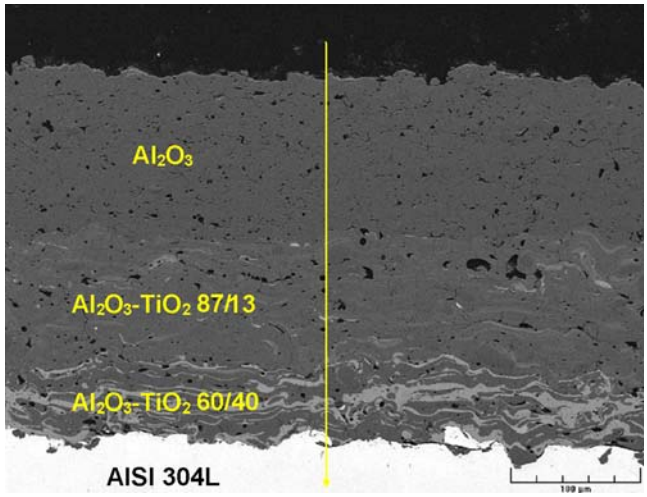


**Fig. 2** Optical micrography of graded alumina-titania without NiAl bond coat

### 2.2 Pore Network Sealing Protocol

The sealing protocol was derived from the studies of Ahmaniemi et al. (Ref 16) and Vippola et al. (Ref 17, 18) considering aluminum phosphate as sealing agent. Aluminum phosphate sealant was prepared from a solution of aluminum hydroxide ($Al(OH)_3$) and orthophosphoric acid ($H_3PO_4$, 85% in weight) diluted with de-ionized water (20% in weight). In such condition, the solution molar P/Al ratio is about 3. The solution was initiated at a temperature of 40 °C on a magnetic stirrer to achieve the exothermic reaction, leading to the formation of the aluminum phosphate, as follows:

$$Al(OH)_3 + 3H_3PO_4 \rightarrow Al(PO_3)_3 + 6H_2O \quad \text{(Eq 1)}$$

This solution was then stored for a released time of 48 h before the sealant was applied manually on the alumina coating surfaces using distemper. The sealing protocol was achieved by a heat treatment adapted from the

studies of Ahmaniemi et al. (Ref 16) and Vippola et al. (Ref 17, 18).

### 2.3 Coating Structural Analysis

**2.3.1 Pore Network Architecture.** The samples were cut parallel to the spray direction using a diamond saw in an oil medium, mounted in rings and infiltrated with epoxy (i.e., impregnation technique). They were polished following standard metallographic techniques (i.e., pre-polishing and diamond slurry polishing) on a semi-automatic polishing system. SEM observations were carried out using the Secondary Electron (SE) mode enhancing the contrast between features. The resolution was 0.14 μm per pixel. Some additional energy dispersive spectroscopic (EDS) analyses were carried out on the samples.

SEM images were discretized and analyzed using Image 1.62 software from NIMH (Research Services Branch of the National Institute of Mental Health, RSB-NIMH, Bethesda, MD, USA).

First, image analysis permitted the quantification of the overall porosity level $V_V$ (i.e., Delesse's protocol (Ref 20)) and the crack network orientation. Pores and cracks were isolated implementing several filtering and morphological protocols. Pores were then analyzed in terms of numbers and relative surface areas, and cracks in terms of cumulated lengths and orientations. Interlamellar (perpendicular to spray direction) and intralamellar (parallel to spray direction) cracks were discriminated and analyzed separately. The cumulated length of cracks per unit surface area, $L_A$ ($m^{-1}$), was calculated to deduce the cumulated surface of cracks per unit volume, $A_V$ ($m^{-1}$), according to the following stereological relationship (Ref 21):

$$A_V = \frac{4}{\pi} L_A \quad \text{(Eq 2)}$$

For each processing parameter set, the results were averaged from 15 fields of view randomly selected across the corresponding polished cross section.

**2.3.2 X-Ray Diffraction.** Phase composition of impregnated alumina coatings were analyzed using X-ray diffractometer (Philips X'Pert, Eindhoven, The Netherlands) (40 kV, 40 mA, CuK$\alpha_1$ radiation at 0.15418 nm) before and after thermal shock and thermal ageing. A 2θ scanning step of 0.017° and a measuring time between each step of 400 s was used to determinate the peak positions of the different phases in the range of $10° < 2\theta < 55°$.

**2.3.3 Mechanical Properties.** Coating Knoop hardness value (KHV) was measured under a 1.962 N load. The longest diagonal of the indenter was aligned parallel to the coating/substrate interface and optical microscopy was used to measure the dimensions of the indent diagonals (with a resolution of about 1 μm). Twelve indentations were performed on random locations on two identical samples. After an adjustment of 10% of the data (i.e., the highest value and the lowest value were discarded), the values were averaged. The apparent coating Young's modulus was then estimated from Marshall's relationship (Ref 22) as follows:

$$E = 0.45 \frac{L}{l} \mathrm{KHV} \quad \text{(Eq 3)}$$

where $L$ represents the Knoop pattern longest diagonal (m), $l$ the shortest one (m), and KHV the Knoop hardness value (KHV), respectively.

### 2.4 Coating Functional Property Protocols

**2.4.1 Dielectric Strength.** The dielectric strength was assessed by measuring the breakdown voltage implementing a dielectrometer developed by CEA and SPCTS. This equipment allows releasing a high alternative voltage, up to 2000 V, at the frequency of 50 Hz at the tip of the electric probe placed in contact with the coating surface under a constant load of 1.962 N. The voltage is progressively increased at a rate of 100 V $s^{-1}$ (Ref 23) until voltage breakdown occurs due to the development of an electric arc between the electric probe tip and the metallic substrate through the ceramic coating. The corresponding current leakage in the circuit is recorded by a micro-amperemeter. For each coating, the test was repeated five times at different locations across the sample coated surface and the resulting breakdown voltage values were averaged.

**2.4.2 Thermal Shocks.** Alumina, phosphate-sealed alumina, and graded alumina-titania coatings were submitted to thermal cycles between 850 and 150 °C using oxyacetylene flame heating and compressed air cooling. The temperature control was achieved by inserting a K-type thermocouple into the drilled hole in the substrate (see Section 2.1) connected to a recording card via a GPIB interface. Temperature measurements were captured every 2 s by the system and the data subsequently analyzed. The breakdown voltage of the tested coating was measured every five thermal cycles until coating degradation (i.e., detectable spallation) occurred.

**2.4.3 Thermal Ageing.** Thermal ageing was carried out only on as-sprayed and phosphate-sealed alumina coatings. Selected samples were disposed in a furnace at atmosphere at 350 °C. The coating breakdown voltages were measured before thermal ageing and then at different intervals of time during ageing: 50, 150, and 400 h.

### 2.5 Statistical Analyses

Average values and standard deviations were determined assuming that the data followed a Gaussian distribution. However, estimation of the variability within the distributions was also performed by calculating the Weibull parameters (Ref 24), i.e., the Weibull modulus, $m$, and the characteristics value, $Xo$, which reflect the data scatter and the 63.2 percentile of the cumulative density. Determination of these parameters was performed by the curve-fitting method (Ref 25).

## 3. Results and Discussion

All as-sprayed and phosphate-sealed ceramic coatings, whatever their composition and architecture, exhibited

breakdown voltages higher than 2000 V, corresponding indeed to the limit of detection of the dielectrometer used in this study.

### 3.1 Alumina As-Sprayed Coating

After thermal ageing tests at 350 °C for 400 h, all coatings showed a breakdown voltage higher than 2000 V except for the architecture A (coating manufactured with fine particle size distribution feedstock of +1 −10 μm). Indeed, the breakdown voltage decreased to 1300 V after 400 h. An electrical loss of about 700 V is considered as very significant. The pore network of this coating series is less adapted to accommodate thermally induced stresses during ageing generating cracks which impede the dielectric strength (Fig. 3).

Thermal shocks between 850 and 150 °C confirmed this fact as well as the poor properties of the graded titania coatings typified as architecture E (Table 3). Thermally shocked graded titania coatings exhibited the worst results with interfacial delamination between layers and a decrease in the breakdown voltage of 700 V after 10 thermal cycles. Multilayered coatings were not compatible with this type of thermal solicitations on account of the multiplication of defective interfaces with the number of intermediate layers.

Concerning the other as-sprayed alumina coatings, only the architecture C revealed a breakdown voltage higher than 2000 V after 50 cycles, synonym of a minimal dielectric strength of 10 kV $mm^{-1}$. The architecture D exhibited similar results with nevertheless a slight decrease to 1900 V in the breakdown voltage. In comparison, architectures A and B sprayed with +1 −10 μm and +5 −45 μm alumina powders, respectively, suffered from significant losses of the electrical insulation after 25 and 30 cycles, respectively.

The electrical insulation is directly dependent on the microstructure of the coating and particularly the thickness, the porosity, and the particle size. All as-sprayed coatings were manufactured with the same thickness of 200 μm, which allowed obtaining an as-sprayed dielectric strength higher than 10 kV $mm^{-1}$ in each case. On the

**Table 3 Measured average breakdown voltages of alumina coatings after thermal shocks between 850 and 150 °C**

| Reference | A | B | C | D | E | F |
|---|---|---|---|---|---|---|
| Number of cycles | 25 | 30 | 50 | 50 | 10 | 15 |
| Average breakdown voltage, V | 1550 | 1800 | >2000 | 1900 | 1300 | 1800 |

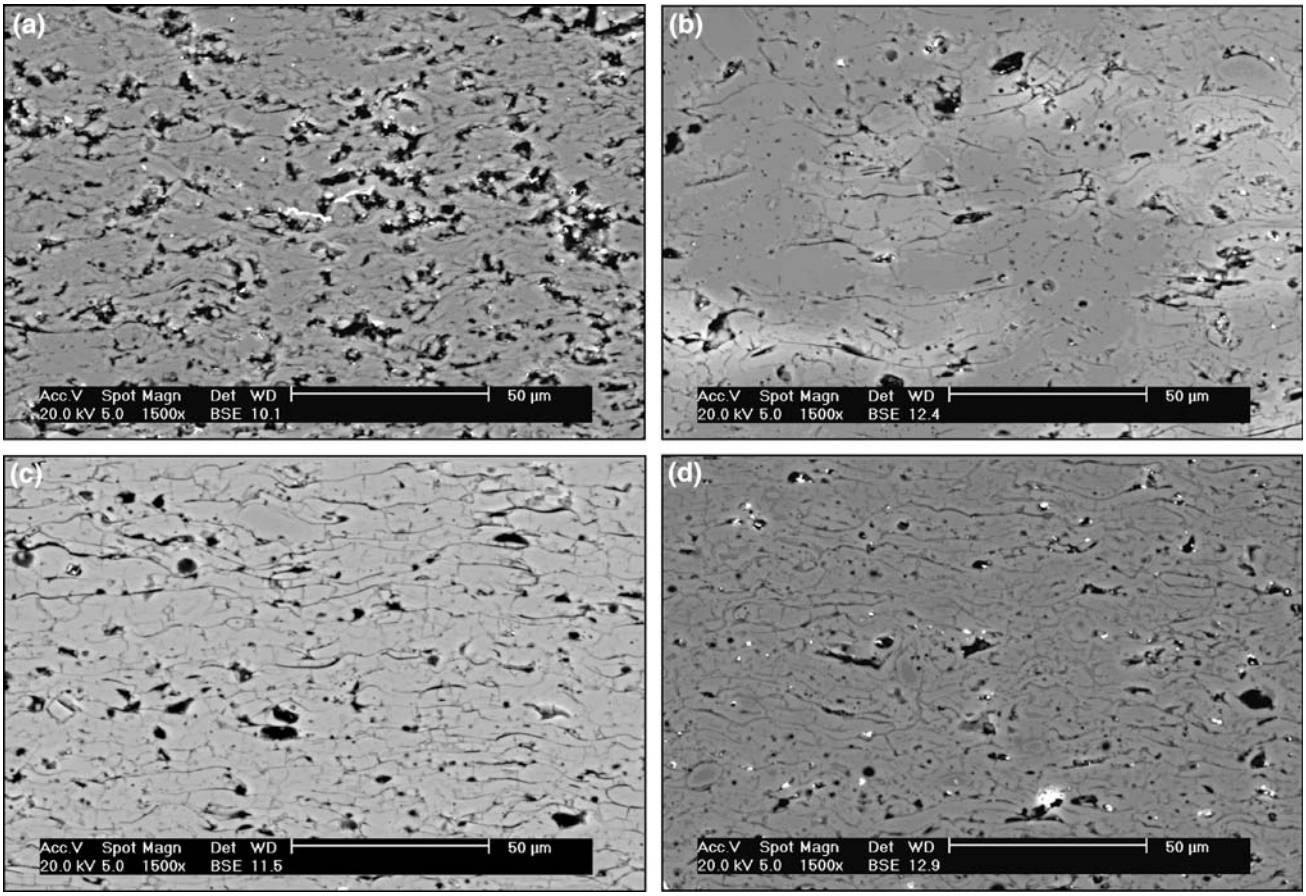


**Fig. 3** Microstructures of as-sprayed coatings after thermal shocks between 850 and 150 °C

other hand, the degree of porosity can be due to cracking process during thermal solicitations, which is directly dependent on the pore network architecture related to the feedstock particle size distributions.

Coating architectures C and D exhibited the best adapted microstructures to sustain thermal stresses resulting from thermal cycling, thanks to a good accommodation toward cracking. Those microstructures allow maintaining almost the integrity of the electrical insulation.

### 3.2 Effect of Aluminum Phosphate Sealing

The aluminum phosphate sealing of alumina coatings permits to form a diffusion barrier against, in particular, the corrosive species by closing the open porosity. In the considered applications, this modification of the microstructure influenced also the thermal, mechanical, and electrical properties of the layers.

If the sealing treatment improved the electrical properties, it rendered also the layers less accommodating to thermal stresses. Indeed, aluminum phosphate sealing leads to bonded coating lamellar structures and induces compressive stresses within the layer which increases its stiffness (Ref 16). It is known that this phenomenon is detrimental to the coating adhesion on its substrate. Nevertheless, coating adhesion was not addressed in the study because the coatings do not undergo mechanical solicitations in the application considered in this study made of a long-term severe ageing (several months at about 400 °C, average temperature, with transient temperatures up to 1500 °C a few times during this period in the presence of a reactive environment made of a complex mixture of acid vapors). Indeed, sealed coatings never pulled-off during long-term ageing, indirectly demonstrating that coating adhesion is not a limiting factor in this case.

In fact, all impregnated coatings are deteriorated after one or two thermal cycles between 850 and 150 °C. These results are very significantly lower when compared to the thermal 50 cycles measured with alumina as-sprayed coatings, particularly for architectures C and D. This phenomenon can be partially explained by a cracking accommodation less efficient than as-sprayed ceramic layers with lamellar microstructure because the crack propagation is not stopped by the pore network. A second phenomenon results from phosphate phase's transitions during thermal cycling: this is why crystalline phases were investigated by XRD analysis.

The as-sprayed alumina coatings show a microstructure composed of a major phase of $\gamma$-$Al_2O_3$ (JCPDS 29-63) and a minor phase of $\alpha$-$Al_2O_3$ (JCPDS 46-1212). In phosphate impregnated alumina coating, these two phases are present too. Nevertheless, other crystalline phases resulting from impregnation are detected and correspond to two other major phases—aluminum orthophosphate $Al(PO_3)_3$ (JCPDS 13-266) and aluminum phosphate type berlinite alpha $\alpha$-$AlPO_4$ (JCPDS 10-423)—and other possible minor phases: cyclohexaphosphate $Al_2P_6O_{18}$ (JCPDS 39-159) and hydrogen aluminum phosphate hydrate $H_2AlP_3O_{10}$, $H_2O$ (JCPDS 48-354) (Fig. 4). The crystallization of aluminum orthophosphate and its polymorphs depends directly on the heat treatment after impregnation and results from the reaction between the sealant and the alumina coating. Indeed, the phosphate bonding to the alumina coating is based both on chemical bonding resulting from the chemical reaction with the alumina coating and on adhesive

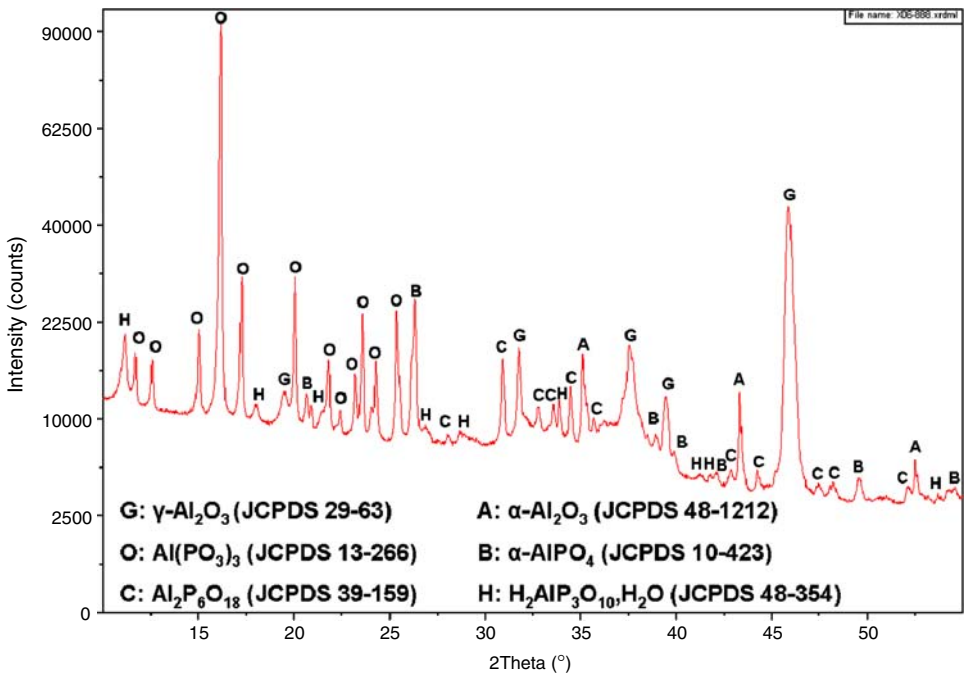


**Fig. 4** Detected phases in impregnated alumina coatings

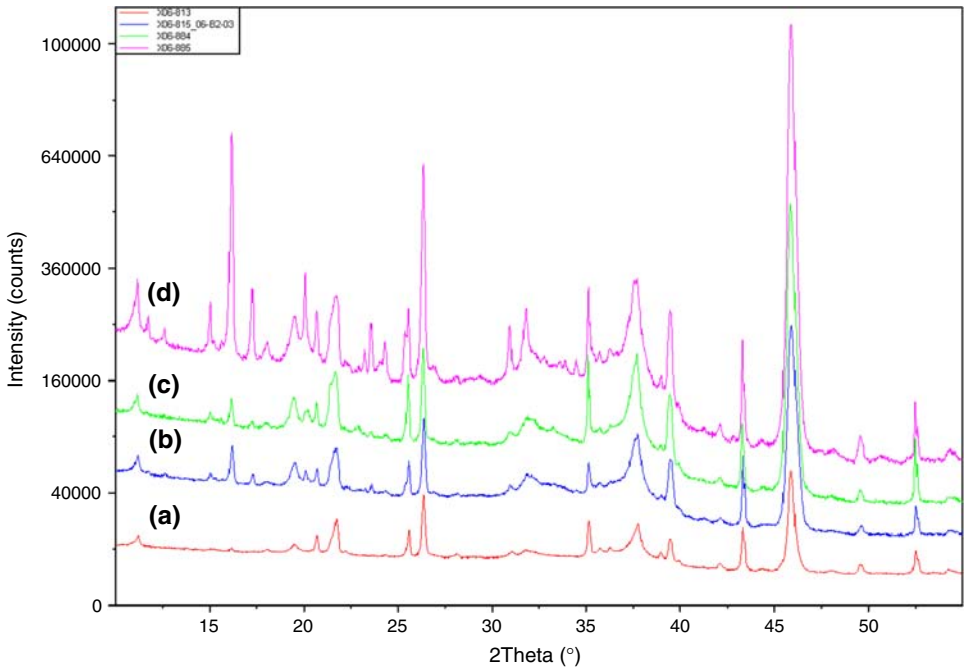


**Fig. 5** Single crystal structure for each sealed alumina coating

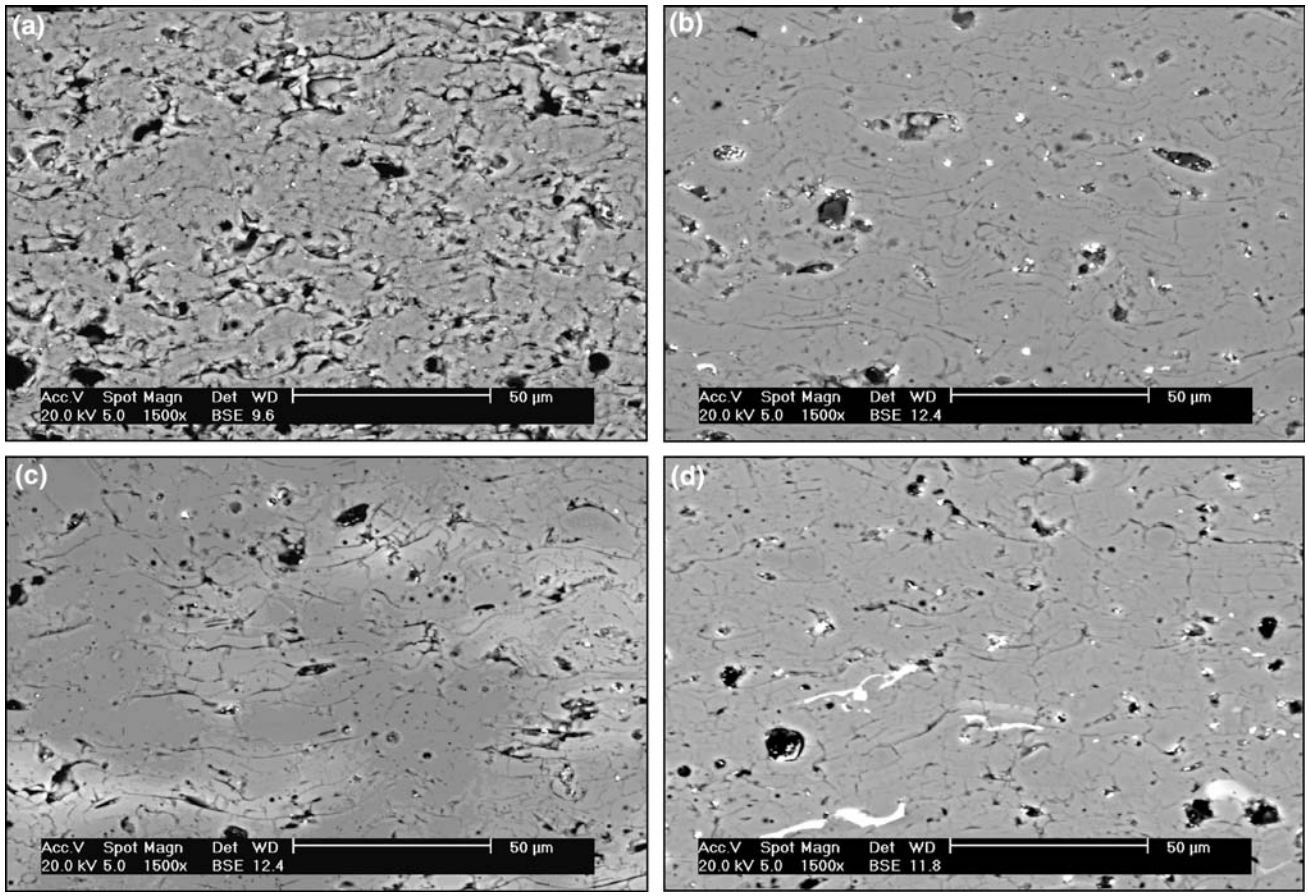


**Fig. 6** Microstructures of sealed coatings after thermal shocks between 650 and 150 °C

binding resulting from the formation of the condensed phosphates in the structural defects of the coating (Ref 17). In this study, each ceramic coating underwent the same impregnation protocol and presented the same phase structure (Fig. 5).

The X-ray data of aluminum orthophosphate and cyclohexaphosphate are very similar and it is difficult to predict which phase is really present. Nevertheless, Vippola et al. (Ref 26) have shown that the major phase is aluminum cyclohexaphosphate.

Another study (Ref 27) indicates an $AlPO_4$ phase transformation with volume variation of berlinite to cristobalite occurring at 778 °C. A hydrated phosphate phase was also identified in the sealed coatings and can degas under thermal cycling between 850 and 150 °C. The rapid degradation of sealed coating may be explained in such a way by the combination of several effects: unaccommodating microstructure face to cracking, induced volume variation by phase transformation, and water degassing.

In order to determine the most adapted architecture face to severe thermal stresses, cyclings between 650 and 150 °C were performed. The microstructures of the alumina coatings are given in Fig. 6. This experiment confirmed the inaptitude of coatings A and B, whose properties are considerably decreased after thermal cycling. As mentioned previously, the architectures C and D possessed the best behavior against high thermal solicitations (Table 4). Estimated heating rates within architecture C and D are different compared to other architectures (Fig. 7). This can be the consequence of a different value of the layer apparent thermal conductivity due to the sealing. In consequence, if one of these sealed coatings should be solicited by thermal ageing with cooling in back face (stainless steel), the architecture D would be the most adapted, thanks to a higher thermal conductivity producing a more efficient dissipation of the heat flux.

### 3.3 Characterization of Impregnated Coatings

The previous hypothesis has been verified by the analysis of the pore architecture of coatings C and D (Table 5). The evolution of the pore network characteristics as a function of the thermal solicitation mode was analyzed after thermal ageing at 350 °C during 400 h (mode 1) and after 10 thermal shocks between 650 and 150 °C (mode 2).

After mode 1, coatings C and D presented similar pore network architecture except a globular porosity two times higher for coating C compared to coating D. On the other hand, coating D is characterized by a higher level of interlamellar microcracks (perpendicular to the spray direction) corresponding very likely to the relaxation of thermal stress by cracking. This fact is inversed in mode 2 where sample C pore network architecture was typified with a higher length of interlamellar microcracks

**Table 4 Measured average breakdown voltages of alumina coatings after thermal shocks between 650 and 150 °C**

| Reference | A | B | C | D |
|---|---|---|---|---|
| Number of cycles | 5 | 10 | 10 | 10 |
| Average breakdown voltage, V | 1300 | >2000 | >2000 | >2000 |
| Remark | Delamination of 3/4 of the coating | Delamination of 1/2 of the coating | Slight delamination at the edges of the coating | No delamination |

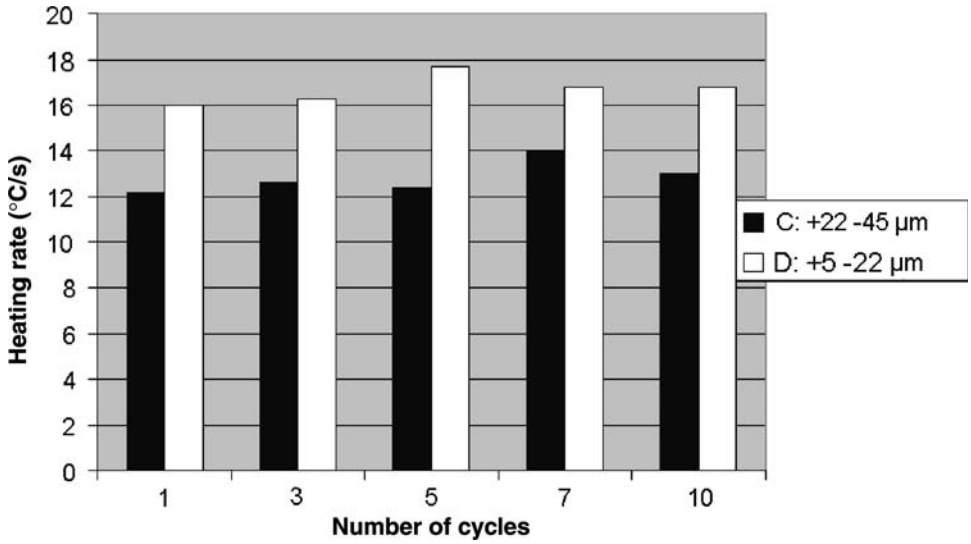


**Fig. 7** Thermal gradient within the sealed coatings C and D during cycling between 650 and 150 °C

**Table 5 Analysis of the porous architecture of the coatings C and D as a function of the thermal solicitation mode (average value and associated standard deviation)**

| | Porosity level ($V_V$), % | Globular pores, % | Cracks, % | Percentage of cracks parallel to substrate interface, % | Percentage of cracks perpendicular to substrate interface, % | $L_A$, mm$^{-1}$ | $S_V$, mm$^{-1}$ |
|---|---|---|---|---|---|---|---|
| Mode 1 | | | | | | | |
| C | 9.9 ± 1.1 | 7.0 ± 0.9 | 3.7 ± 0.4 | 71.1 ± 2.0 | 28.9 ± 2.0 | 9.4 ± 1.3 | 3.8 ± 0.6 |
| D | 8.4 ± 0.8 | 3.2 ± 0.2 | 5.5 ± 0.7 | 89.7 ± 1.4 | 10.3 ± 1.4 | 15.9 ± 2.2 | 1.8 ± 0.3 |
| Mode 2 | | | | | | | |
| C | 13.4 ± 2.1 | 6.5 ± 1.3 | 7.9 ± 1.0 | 83.2 ± 1.5 | 16.8 ± 1.5 | 26.7 ± 4.2 | 5.3 ± 0.9 |
| D | 6.0 ± 0.3 | 2.8 ± 0.3 | 3.4 ± 0.3 | 86.2 ± 1.3 | 13.8 ± 1.3 | 9.9 ± 0.9 | 1.6 ± 0.2 |

**Table 6 Mechanical properties of sealed coatings C and D as a function of the thermal solicitation mode**

| Reference | KHV, GPa | *E*, GPa | Weibull modulus |
|---|---|---|---|
| Mode 1 | | | |
| C | 8.5 ± 0.6 | 35 ± 2 | 9.5 |
| D | 8.9 ± 0.7 | 34 ± 3 | 6.3 |
| Mode 2 | | | |
| C | 8.7 ± 0.9 | 34 ± 3 | 4.6 |
| D | 8.2 ± 0.7 | 35 ± 3 | 7.6 |

(26.7 mm$^{-1}$) and by a total pore level about twice of the one of architecture D. This specificity can explain the delamination observed at the edges of the coatings after 10 cycles due to the poor accommodation of the thermal stresses by the microstructure. It is important to remark also that coating C in mode 1 presents a significantly higher intralamellar microcracks (parallel to the spray direction) ratio (about three times higher than coating D in same mode): this is not compatible with the property of a diffusion barrier.

Therefore, the choice of the initial particle size is very important for the final thermal and electrical properties of the alumina coating. Concerning the mechanical properties, the architectures C and D do not have significant influences on the values of the apparent layer elastic modulus (Table 6).

## 4. Conclusion

Alumina coatings were manufactured by plasma spraying using different particle size distributions in order to protect stainless steel AISI 304L structures in some extreme environments encountered, for example, in nuclear waste processing (long-term ageing, about 300 °C for several months, coupled to thermal shocks with numerous cycles up to 850 °C for a few seconds and a few ones up to 1500 °C during this period under a reactive environment made of a complex mixture of acid vapors in the presence of an electric field of a few hundred volts and a radioactive activity higher than 10 MGy on a cumulated period of 4 years).

Aluminum phosphate impregnation appeared to be an efficient post-treatment to fill connected porosity of these coatings. They exhibit typical microstructural characteristics of plasma-sprayed ceramics such as important ratios of globular porosity and microcracks after thermal solicitations.

Their behavior was directly dependent on the architecture of the as-sprayed open porosity network which was dependent on the particle size distribution. Alumina as-sprayed coatings manufactured with +22 −45 μm and +5 −20 μm particle size distributions exhibit good dielectric strengths after thermal solicitations compared to the ones manufactured with +1 −10 μm and +5 −45 μm particle size distributions or to graded titania coatings. These results were attributed to higher accommodating microstructures in front of thermal solicitations. Indeed, the evolution of the electrical insulation of these sealed ceramic coatings is sensitive to the degradation of the microstructure.

## References


1. C.W. Mossor, "Electrical Breakdown of Thermal Spray Alumina Ceramic Applied to AlSiC Base Plates Used in Power Modules Packaging," Ph.D. Thesis, Faculty of Virginia Polytechnic Institute, Virginia, 1999
2. A. Kulkarni, J. Gutleber, S. Sampath, A. Goland, W.B. Lindquist, H. Herman, A.J. Allen, and B. Bowd, Studies of the Microstructure and Properties of Dense Ceramic Coatings Produced by High-Velocity Oxygen-Fuel Combustion Spraying, *Mater. Sci. Eng. A*, 2004, **369**, p 124-137
3. S. Beauvais, "Etude de l'influence de la porosité sur les propriétés électriques de dépôts réalisés par projection plasma (Influence of the Porosity of Electric Properties of Plasma-Sprayed Deposits)," Ph.D. Thesis, Ecole des Mines de Paris, Paris, 2003, in French
4. O. Sarikaya, Effect of Some Parameters on Microstructure and Hardness of Alumina Coatings Prepared by the Air Plasma Spraying Process, *Surf. Coat. Technol.*, 2005, **190**, p 388-393
5. O. Sarikaya, Effect of the Substrate Temperature on Properties of Plasma Sprayed $Al_2O_3$ Coatings, *Mater. Des.*, 2005, **26**, p 53-57
6. A. Portinha, V. Teixeira, J. Carneiro, J. Martins, M.F. Costa, R. Vassen, and D. Stoever, Characterization of Thermal Barrier Coatings with a Gradient in Porosity, *Surf. Coat. Technol.*, 2005, **195**, p 245-251
7. N.H. Menzler, M. Bram, H.P. Buchkremer, and D. Stöver, Development of a Gastight Sealing Material for Ceramic Components, *J. Eur. Ceram. Soc.*, 2003, **23**, p 445-454
8. G. Antou, "Améliorations de revêtements barrières thermiques par un procédé de refusion laser in-situ utilisant un laser à diodes (Improvements of Thermal Barrier Coatings by an In-situ Laser Remelting Process Using Diode Laser)," Ph.D. Thesis, University Louis Pasteur – Strasbourg I, Strasbourg, 2004, in French
9. G. Bolelli, V. Cannillo, C. Lugli, L. Lusvarghi, and T. Manfredini, Plasma-Sprayed Graded Ceramic Coatings on Refractory Materials for Improved Chemical Resistance, *J. Eur. Ceram. Soc.*, 2006, **26**(13), p 2561-2579

10. D.P. Monaghan, D.G. Teer, P.A. Logan, K.C. Laing, R.I. Bates, and R.D. Arnell, An Improved Method for the Deposition of Corrosion-Resistant Aluminum Coatings for Aerospace Applications, *Surf. Coat. Technol.*, 1993, **60**(1-3), p 592-596
11. R. Krishnan, S. Dash, R. Kesavamoorthy, C.B. Rao, A.K. Tyagi, and B. Raj, Laser Surface Modification and Characterization of Air Plasma Sprayed Alumina Coatings, *Surf. Coat. Technol.*, 2006, **200**(8), p 2791-2799
12. T. Zhang, Z. Qiu, Y. Bao, D.T. Gawne, and K. Zhang, Temperature Profiles and Thermal Stress Analysis of Plasma Sprayed Glass-Composite Coatings, *Thermal Spray: Surface Engineering via Applied Research,* C.C. Berndt, Ed., Materials Park, OH, ASM International, 2000, p 355-361
13. S. Liscano, L. Gil, and M.H. Staia, Effect of Sealing Treatment on the Corrosion Resistance of Thermal-Sprayed Ceramic Coatings, *Surf. Coat. Technol.*, 2004, **188-189**, p 135-139
14. R. Westergard and S. Hogmark, Sealing to Improve the Wear Properties of Plasma Sprayed Alumina by Electro-Deposited Ni, *Wear*, 2004, **256**(11-12), p 1153-1162
15. H.J. Kim, S. Odoul, C.H. Lee, and Y.G. Kweon, The Electrical Insulation Behavior and Sealing Effects of Plasma-Sprayed Alumina–Titania Coatings, *Surf. Coat. Technol.*, 2001, **140**(3), p 293-301
16. S. Ahmaniemi, M. Vippola, P. Vuoristo, T. Mäntylä, M. Buchmann, and R. Gadow, Residual Stresses in Aluminum Phosphate Sealed Plasma Sprayed Oxide Coatings and Their Effect on Abrasive Wear, *Wear*, 2002, **252**(7-8), p 614-623
17. M. Vippola, S. Ahmaniemi, J. Keränen, P. Vuoristo, T. Lepistö, T. Mäntylä, and E. Olsson, Aluminum Phosphate Sealed Alumina Coating: Characterization of Microstructure, *Mater. Sci. Eng. A*, 2002, **323**(1-2), p 1-8
18. M. Vippola, J. Vuorinen, P. Vuoristo, T. Lepistö, and T. Mäntylä, Thermal Analysis of Plasma Sprayed Oxide Coatings Sealed with Aluminium Phosphate, *J. Eur. Ceram. Soc.*, 2002, **22**(12), p 1937-1946
19. ISO 13565-1/Cor 1:1998 (Geometrical Products Specifications (GPS) – Surface Texture: Profile Method – Part 1: Filtering and General Measurement Conditions) and ISO 13565-2/Cor 1:1998 (Geometrical Products Specifications (GPS) – Surface Texture: Profile Method – Part 2: Height Characterization Using the Linear Material Ratio Curve) Standards
20. A. Delesse, Procédé mécanique pour déterminer la composition des roches (Mechanical Process to Determine the Composition of Rocks), *Annales des Mines*, 1848, 13, p 379-388, in French
21. E.E. Underwood, Stereology, or the Quantitative Evaluation of Microstructures, *J. Micros.*, 1969, **89**(2), p 161-180
22. D.B. Marshall, T. Noma, and A.G. Evans, A Simple Method for Determining Elastic Modulus to Hardness Ratios Using Knoop Indentation Measurements, *J. Am. Ceram. Soc.*, 1982, **65**, p 175-176
23. NF EN 60243-1:1998, ''Rigidité diélectrique des matériaux isolants – Méthodes d'essai – Partie 1: Essais aux fréquences industrielles (Dielectric Strength of Insulating Materials – Test Methods – Part 1: Tests at Power Frequencies)'', in French
24. P. Ostojic and C.C. Berndt, Variability in Strength of Thermally Sprayed Coatings, *Surf. Coat. Technol.*, 1988, **34**, p 43-50
25. L. Devore, Probability and Statistics for Engineering and the Sciences, (3rd ed.). Brooks-Cole Publishing Company, Pacific Grove, CA, 1991, p 542
26. M. Vippola, J. Keränen, X. Zou, S. Hovmöller, T. Lepistö T. Mäntylä, Structural Characterization of Aluminum Phosphate Binder, *J. Am. Ceram. Soc.*, 2000, **83**(7), p 1834-1836
27. W. Zhenjie and Y. Danian, An Investigation of the Phase Transformation of $AlPO_4$ at High Pressure and High Temperature, *Scient. Geol. Sin.*, 1990, **3**, p 287-293